Neuroendocrinology Letters Volume 47 No. 5 2026
ISSN: 0172-780X; ISSN-L: 0172-780X; Electronic/Online ISSN: 2354-4716
Web of Knowledge / Web of Science: Neuroendocrinol Lett
Pub Med / Medline: Neuro Endocrinol Lett

ORIGINAL ARTICLE

Identification of Key Regulatory Genes Involved in Pyroptosis in Osteoarthritis Through Integrated Single-Cell Transcriptomic and Machine Learning Analysis

Jun-Lin Chen[1], Yan-Hui Suo[1], Rui-Hai Yan[2]

1 Department of Orthopedics, Handan Central Hospital, Handan 056001, China
2 Emergency Department, Handan Central Hospital, Handan 056001, China

Correspondence to: Rui-Hai Yan, BM
Emergency Department, Handan Central Hospital, No. 15, Zhonghua South Street, Hanshan District, Handan 056001, China
tel.: +86 19833063301; e-mail: yanruihaiyrhcd@126.com

Submitted: 2026-04-08 *Accepted: 2026-07-07* *Published online: 2026-08-15*

Key words: **machine learning; osteoarthritis; pyroptosis; single-cell; WGCNA**

Neuroendocrinol Lett 2026; **47**(5):304–316 **PMID:** 42647555 470502 • **www.nel.edu**

Abstract

OBJECTIVE: This study aimed to identify pyroptosis related genes (pyroptosis RGs) in osteoarthritis (OA) and to evaluate their potential as candidate biomarkers by integrating bulk transcriptomic analysis, machine learning, and single cell RNA sequencing.

METHODS: Bulk RNA sequencing datasets (GSE55235 and GSE55457) and a single cell RNA sequencing dataset (GSE216651) related to OA were obtained from the Gene Expression Omnibus database, and gene sets associated with OA and pyroptosis were retrieved from GeneCards. Differential expression analysis and weighted gene co expression network analysis (WGCNA) of GSE55235 were used to derive differentially expressed pyroptosis related genes (DEPRGs). Candidate hub genes were screened by intersecting rankings from five cyto-Hubba algorithms with three supervised machine learning models (least absolute shrinkage and selection operator, support vector machine–recursive feature elimination, and random forest), and their diagnostic performance was evaluated using receiver operating characteristic curve analysis in the training and validation cohorts. The potential biological roles of the identified hub genes were further examined through functional enrichment analysis, immune cell infiltration assessment, and single-cell transcriptomic profiling.

RESULTS: Twenty-one DEPRGs were identified. Among these, interleukin 8 (CXCL8) and NF kappa B inhibitor alpha (NFKBIA) emerged as central hub genes with consistent diagnostic performance across cohorts. Functional enrichment analyses indicated that these genes are primarily implicated in inflammatory signaling and immune regulation pathways, including responses to tumor necrosis factor and lipopolysaccharide, chemokine and cytokine activity, and Toll like receptor, TNF, and IL 17 signaling. Single-cell transcriptomic analysis demonstrated predominant expression of CXCL8 and NFKBIA in synovial macrophages. In these cells, expression of both genes was positively correlated with pyroptosis scores, and macrophages displayed the highest pyroptosis activity among the analyzed synovial cell populations in OA.

CONCLUSION: CXCL8 and NFKBIA were identified as synovium associated pyroptosis related genes in OA with promising diagnostic performance in public datasets. These in silico findings refine current understanding of OA related inflammatory pathways and generate hypotheses for future mechanistic and experimental studies.

INTRODUCTION

Osteoarthritis (OA) represents the most prevalent joint disorder and is a major contributor to pain, joint dysfunction, and disability. With progressive population aging worldwide, osteoarthritis already affects a very large and growing proportion of the population, and demographic trends suggest that the number of affected individuals will continue to rise substantially over the coming decades (Siddiq *et al.* 2024; Expert Group for Osteoarthritis Guidelines, 2024; Glyn-Jones *et al.* 2015). Beyond its clinical manifestations, OA markedly diminishes quality of life in affected individuals and is associated with a substantial healthcare and societal burden, as highlighted by epidemiological and review studies (Glyn-Jones *et al.* 2015; Litwic *et al.* 2013). Early-stage diagnosis remains difficult, and current therapeutic strategies are largely confined to symptomatic pharmacologic management and joint arthroplasty. Effective disease-modifying interventions capable of halting or slowing structural progression remain limited (Chen and Song, 2025; Yu and Wang, 2025). In this context, clarification of the molecular mechanisms driving OA initiation and progression, together with the identification of potential therapeutic targets, is of considerable clinical relevance.

From a pathological perspective, OA is characterized by progressive degeneration of articular cartilage, remodeling of subchondral bone, accompanied by synovial inflammation, and osteophyte formation (Cui *et al.* 2025). Among these pathological alterations, synovial inflammation and immune cell dysregulation have emerged as critical contributors to both disease onset and progression (Shen and Jiang, 2025; Sanchez-Lopez and Coras, 2022; Motta *et al.* 2023; Mathiessen and Conaghan, 2017).

Pyroptosis, a form of programmed cell death, initiates inflammatory cascades through the release of pro-inflammatory cytokines, including interleukin-1β (IL-1β) and interleukin-18 (IL-18) (Qi *et al.* 2024; Vasudevan *et al.* 2023). Increasing evidence has demonstrated a close association between synovial pyroptosis and OA pathogenesis (Kuang *et al.* 2024). Nevertheless, systematic analyses integrating multiple transcriptomic datasets to delineate the contribution of pyroptosis to OA remain limited. Accordingly, identifying pyroptosis related candidate biomarkers in OA using available high throughput data is of particular significance. This study was designed to explore key pyroptosis related genes (pyroptosis RGs) in OA synovial tissue and to prioritize candidate diagnostic and mechanistic targets through an integrated analytical framework combining bulk and single cell transcriptomics with machine learning algorithms.

MATERIALS AND METHODS

Acquisition of public datasets

Ribonucleic acid (RNA) sequencing datasets associated with OA, including GSE55235 and GSE55457 (synovial

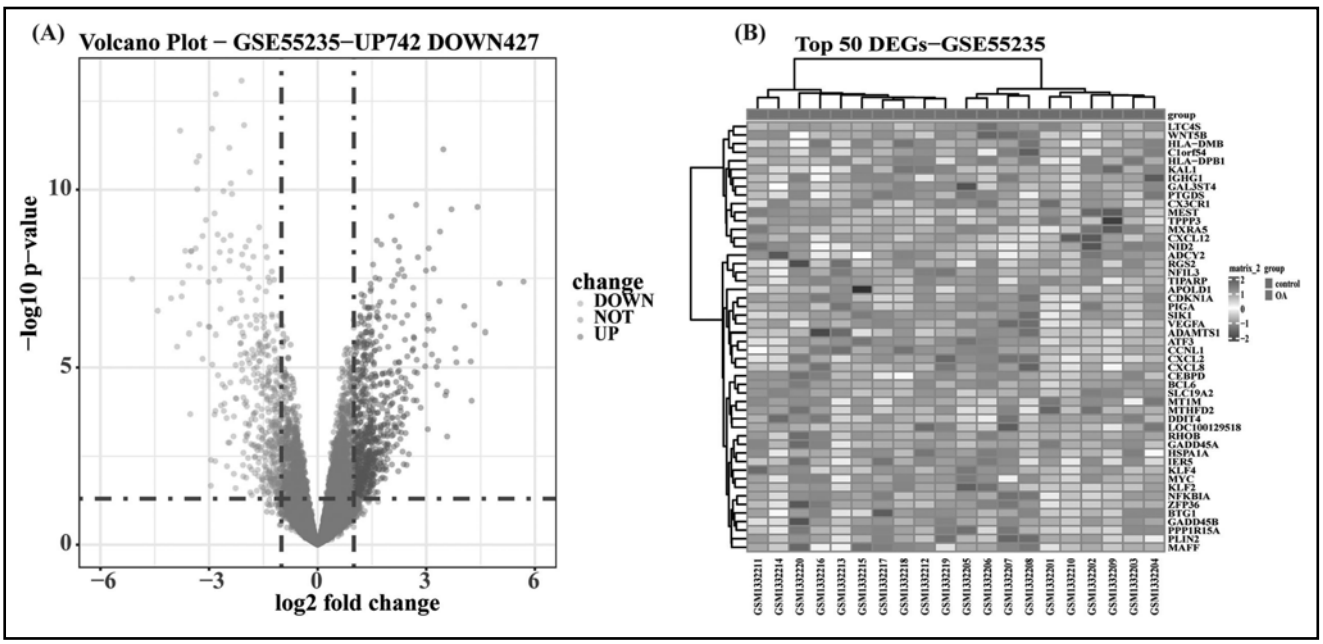

Fig. 1. Differentially expressed genes in the GSE55235 osteoarthritis training cohort
(A) Volcano plot showing differentially expressed genes between osteoarthritis and control synovial tissue samples in GSE55235. (B) Heatmap showing the expression patterns of representative differentially expressed genes across samples.

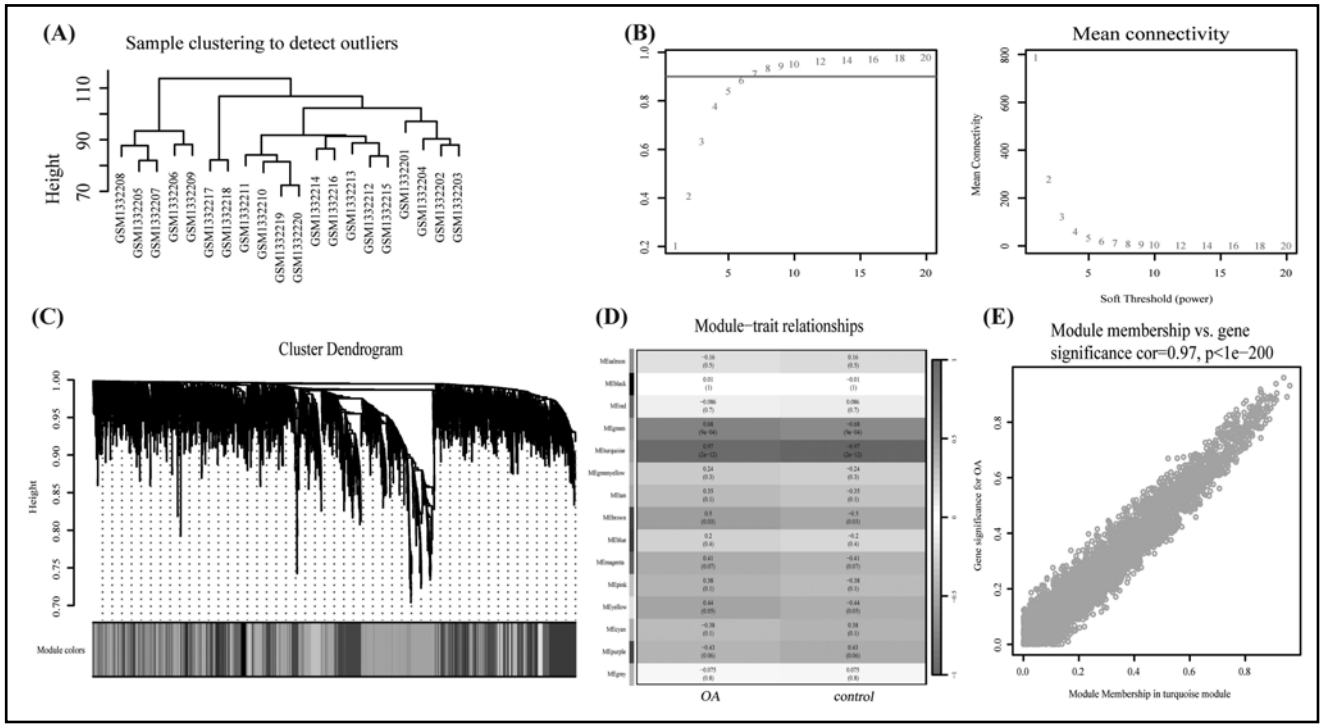

Fig. 2. Weighted gene co-expression network analysis in GSE55235
(A) Hierarchical clustering dendrogram of samples in GSE55235. (B) Analysis used to determine the soft-thresholding power for network construction. (C) Gene dendrogram with module color assignment. (D) Heatmap showing correlations between module eigengenes and osteoarthritis status. (E) Scatter plot of module membership versus gene significance for the turquoise module.

tissue from OA and control samples), as well as single-cell RNA sequencing data of synovial cells (GSE216651), were retrieved from the Gene Expression Omnibus (GEO) database. The GSE55235 dataset was designated as the training cohort, whereas GSE55457 was used as the validation cohort. Genes related to osteoarthritis (OA-RGs) and pyroptosis (Pyroptosis-RGs) were retrieved from the GeneCards database.

Differential expression analysis

Differential gene expression between OA synovial tissue and normal synovial tissue was analyzed using the limma package in R software. Genes meeting the criteria of adjusted p-value < 0.05 (Benjamini–Hochberg correction) and $|\log2FC| \geq 1$ were considered differentially expressed. Volcano plots and heatmaps were generated to visualize the results.

Weighted gene co-expression network analysis

Prior to network construction, sample clustering was performed to identify and exclude outliers. A soft thresholding power ($\beta = 7$) was selected to approximate scale free network topology (scale free topology fit index ≈ 0.9). Based on this parameter, an adjacency matrix was generated and subsequently converted into a topological overlap matrix. Gene dissimilarity was calculated, followed by hierarchical clustering to identify gene modules, with the minimum module size set to 30 genes. Correlations between module eigengenes and the phenotypic trait of interest (OA) were subsequently calculated to determine the modules most strongly associated with disease status.

Identification and functional annotation of differentially expressed pyroptosis-RGs

Pyroptosis-RGs and OA-RGs retrieved from the GeneCards database were intersected with the differentially expressed genes identified in the GSE55235 dataset and with the gene modules most strongly correlated with OA in the weighted gene co-expression network analysis (WGCNA). This integrative approach yielded differentially expressed pyroptosis-related genes (DEPRGs) associated with OA.

To characterize their potential biological roles, Gene Ontology (GO) functional annotation and Kyoto Encyclopedia of Genes and Genomes (KEGG) pathway enrichment analyses were subsequently conducted for the identified DEPRGs.

Screening of hub genes using machine learning algorithms

Protein–protein interaction networks were constructed using the STRING database and visualized with Cytoscape software. To prioritize candidate genes, five algorithms implemented in the cytoHubba plugin—maximal clique centrality (MCC), maximum neighborhood component (MNC), degree, stress, and betweenness—were applied.

Subsequently, three machine-learning algorithms—least absolute shrinkage and selection operator

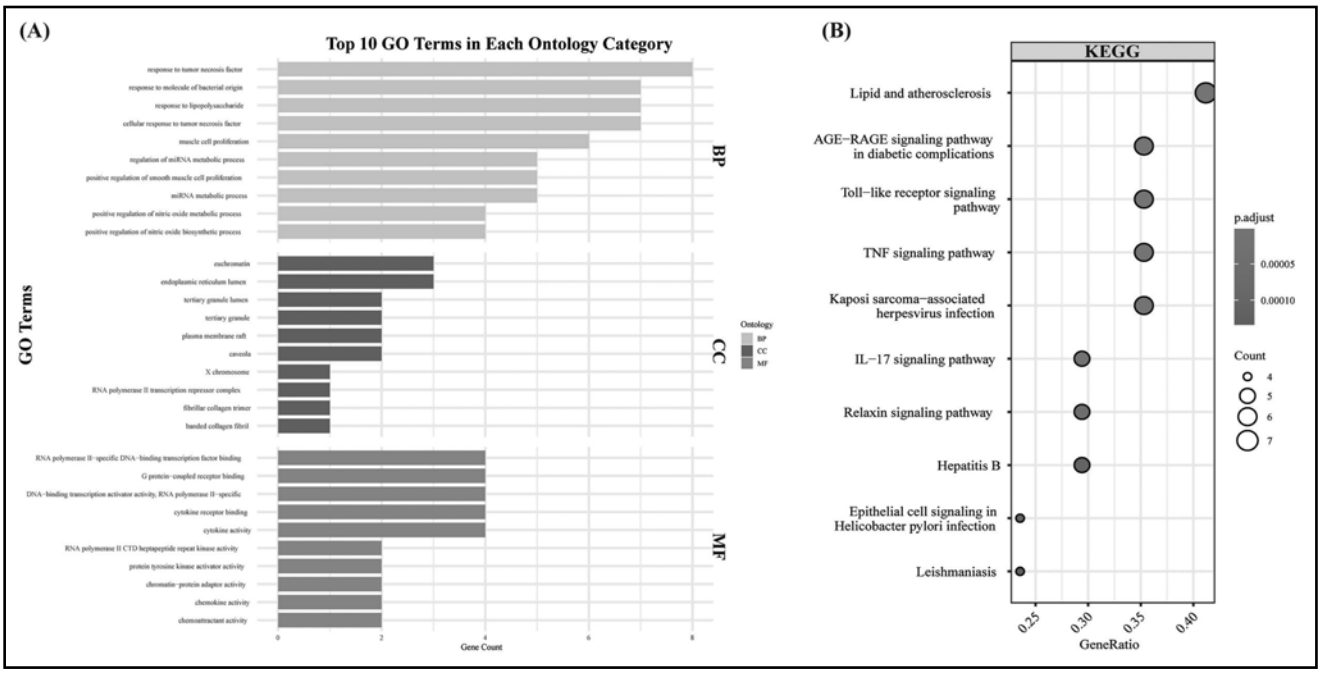

Fig. 3. GO and KEGG enrichment analysis of differentially expressed pyroptosis-related genes
(A) Gene Ontology enrichment analysis of the differentially expressed pyroptosis-related genes. (B) Kyoto Encyclopedia of Genes and Genomes pathway enrichment analysis of the differentially expressed pyroptosis-related genes.

(LASSO), support vector machine–recursive feature elimination (SVM RFE), and random forest (RF)—were applied to the candidate genes to identify diagnostic biomarkers for OA and to determine the final hub genes based on cross validated feature importance and classification performance.

Expression patterns and diagnostic performance of hub genes

Hub gene expression levels in OA and normal synovial tissue samples were compared in the training cohort using box plot visualization, followed by validation in the independent testing cohort. Receiver operating characteristic (ROC) curve analysis was conducted in both datasets to evaluate diagnostic performance. Genes demonstrating an area under the curve (AUC) value greater than 0.7 in both the training and validation cohorts were considered to have promising diagnostic performance in these datasets and were retained as candidate biomarkers.

Gene set enrichment analysis and immune infiltration analysis of hub genes

Within the GSE55235 training cohort, samples were stratified into high- and low-expression groups based on the expression levels of the identified hub genes. Gene set enrichment analysis (GSEA) was subsequently performed to explore associated biological pathways, using nominal p value < 0.05 and false discovery rate < 0.25 as significance thresholds. Immune cell infiltration was estimated using the CIBERSORT algorithm, and cell types with $p < 0.05$ in CIBERSORT output were retained for downstream comparisons.

Processing and annotation of single-cell RNA sequencing data

The single-cell RNA sequencing (scRNA-seq) dataset GSE216651 was processed using the Seurat package in R. Quality control filtering was performed as follows: cells expressing < 400 or > 6,000 genes and cells with a mitochondrial gene proportion > 20% were excluded.

Following quality control, data were normalized and batch effects were corrected based on the top 2,000 highly variable genes. Principal component analysis was then performed, statistically significant principal components were used for clustering at a resolution of 0.8, and uniform manifold approximation and projection (UMAP) was applied for visualization. Cell types were annotated using previously published references and the CellMarker database.

Correlation between hub genes and pyroptosis scores in single-cell data

Hub gene expression across annotated cell populations was visualized using violin plots. The pyroptosis-related gene set was obtained from the MSigDB database, and the AddModuleScore function was applied to calculate pyroptosis scores for individual cells based on this predefined gene set. UMAP projections and violin plots were generated to depict the

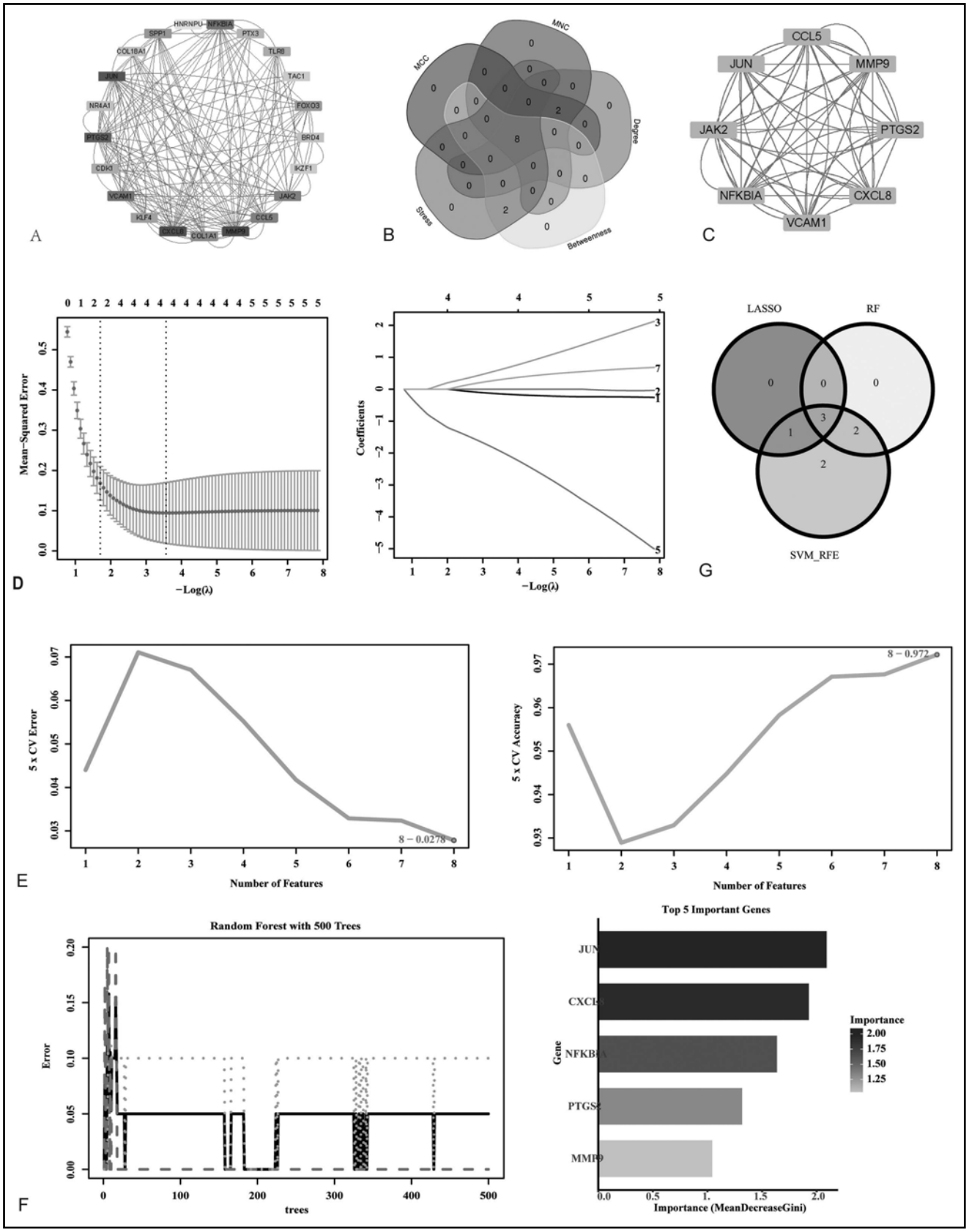

Fig. 4. Identification of hub genes by network and machine-learning analyses
(A) Protein-protein interaction network of the differentially expressed pyroptosis-related genes. (B) Overlap of top-ranked genes identified by five cytoHubba algorithms. (C) Network visualization of the overlapping candidate genes. (D) Least absolute shrinkage and selection operator analysis. (E) Support vector machine-recursive feature elimination analysis. (F) Random forest analysis. (G) Overlap of hub genes identified by the three machine-learning methods.

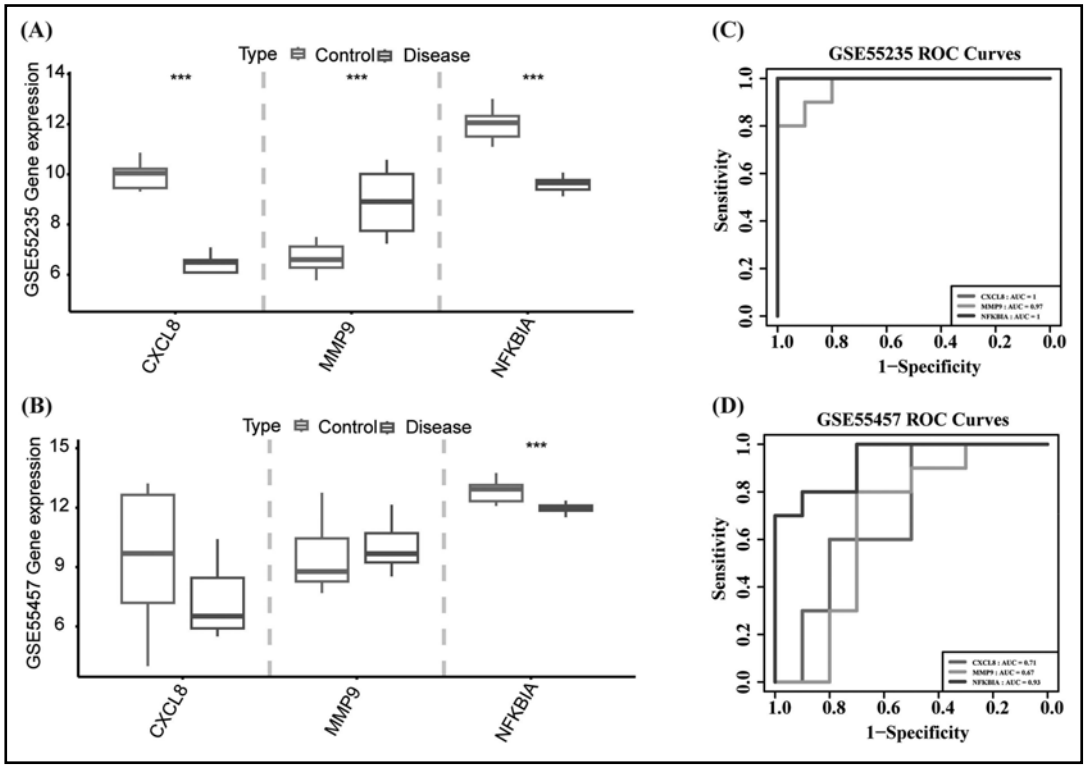

Fig. 5. Expression and diagnostic performance of hub genes in bulk RNA sequencing datasets (A) Expression levels of hub genes in the GSE55235 training cohort. (B) Expression levels of hub genes in the GSE55457 validation cohort. (C) Receiver operating characteristic curves of hub genes in GSE55235. (D) Receiver operating characteristic curves of hub genes in GSE55457.

distribution of pyroptosis activity across different cell types. In addition, pyroptosis scores were compared between OA and control samples using violin plot visualization.

Cell types exhibiting significantly elevated pyroptosis activity were selected as subsets for subsequent analysis. Within these subsets, hub gene expression patterns were examined, and correlations between hub gene expression levels and pyroptosis scores were systematically evaluated.

Statistical analysis

All data preprocessing and statistical analyses of GEO datasets were performed using R software. Continuous variables were compared between two groups according to their data distribution. Variables consistent with a normal distribution were analyzed using an independent-samples t-test, whereas non-normally distributed variables or count data were assessed using the Wilcoxon rank-sum test. Correlation analyses were performed using Pearson or Spearman methods according to data distribution. All statistical tests were two sided, and $p < 0.05$ was considered statistically significant after adjustment where applicable.

RESULTS

Screening of differentially expressed genes in OA

In the GSE55235 training cohort, differential expression analysis identified 1,169 DEGs between OA and normal synovial tissue samples, including 742 upregulated and 427 downregulated genes (Figures 1A, 1B).

Construction of the WGCNA weighted network

Following hierarchical clustering, all 20 samples from the GSE55235 dataset met quality control criteria and were included in subsequent analyses (Figure 2A). The soft-thresholding power (β) was determined to be 7, achieving a scale-free topology fit index of 0.9 (Figure 2B).

A total of 15 gene co-expression modules were identified. Among these, the turquoise module (968 genes) showed the strongest positive correlation with OA status (module eigengene–trait correlation $r = 0.97$, $p < 0.001$) and was selected as the key module for downstream analyses (Figures 2C–E).

Identification and functional annotation of DEPRGs

An intersection analysis was performed among 877 Pyroptosis-RGs, 6,521 OA-RGs, 1,169 DEGs identified from GSE55235, and 968 genes within the key turquoise module derived from WGCNA. This four way intersection yielded 21 DEPRGs associated with OA that were carried forward to functional enrichment and network analyses.

GO and KEGG pathway enrichment analyses were subsequently performed for these 21 DEPRGs (Figures 3A, 3B). GO analysis suggested involvement in multiple biological processes, including response to tumor necrosis factor (TNF), response to molecules of bacterial origin, and response to lipopolysaccharide. In terms of cellular components, enrichment was observed primarily in the endoplasmic reticulum lumen, euchromatin, fibrillar collagen trimer, and banded collagen fibril. Molecular function analysis indicated significant

enrichment in chemokine activity, cytokine activity, cytokine receptor activity, and G protein-coupled receptor binding. KEGG pathway analysis further demonstrated associations with the Toll-like receptor, TNF, and interleukin-17 (IL-17) signaling pathways, among others.

Screening of hub genes using machine learning algorithms

A protein-protein interaction network (PPI) comprising the DEPRGs was constructed using the STRING database and subsequently visualized with Cytoscape software. Within the network, darker node coloration represented greater connectivity and higher interaction density (Figure 4A).

The top ten DEPRGs ranked by five CytoHubba algorithms—MCC, MNC, degree, stress, and betweenness—were compared, and their intersection yielded eight overlapping candidate genes (Figure 4B). These genes included interleukin-8 (CXCL8), matrix metallopeptidase 9 (MMP9), Jun Proto-Oncogene, prostaglandin-endoperoxide synthase 2, vascular cell

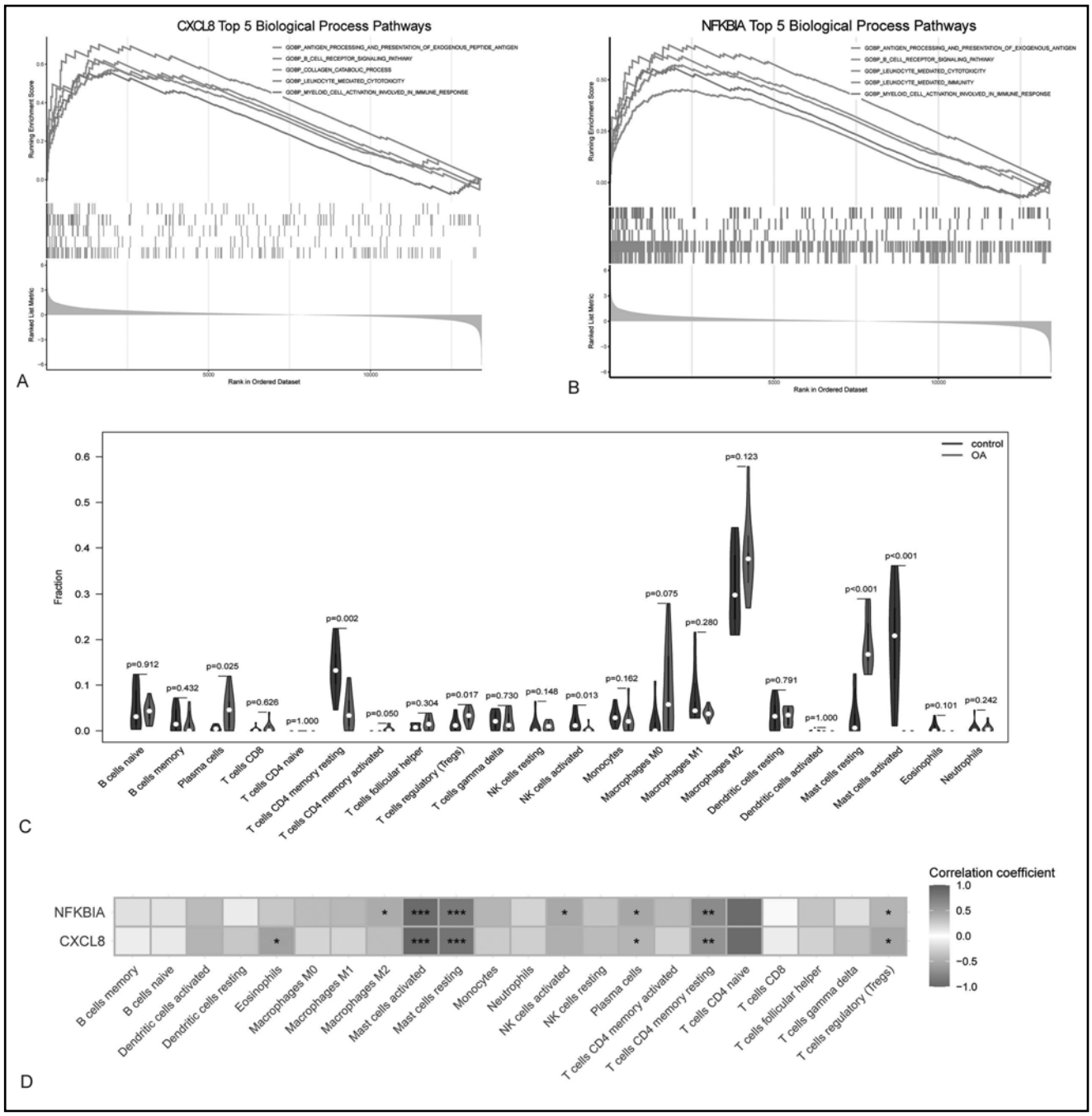

Fig. 6. GSEA and immune infiltration analyses of CXCL8 and NFKBIA
(A) Gene set enrichment analysis plot for CXCL8. (B) Gene set enrichment analysis plot for NFKBIA. (C) Distribution of immune-cell subsets in osteoarthritis and control samples estimated by CIBERSORT. (D) Heatmap showing correlations between hub gene expression and immune-cell subsets.

adhesion molecule 1, NF-kB inhibitor alpha (NFKBIA), Janus kinase 2, and C-C motif chemokine ligand 5 (Figure 4C).

To further refine candidate biomarkers, three machine learning algorithms—LASSO, SVM-RFE, and RF—were applied to these eight genes. Both LASSO and SVM-RFE employed five-fold cross-validation. LASSO identified four genes as candidate diagnostic biomarkers for OA (Figure 4D). The SVM-RFE model demonstrated optimal performance when eight feature genes were included (Figure 4E). Using the RF algorithm, genes with importance scores > 1 among the top five ranked features were retained as candidate diagnostic biomarkers (Figure 4F).

Integration of the three machine learning approaches identified three overlapping hub genes—CXCL8, MMP9, and NFKBIA—which were subsequently evaluated for diagnostic performance (Figure 4G).

Diagnostic performance of hub genes

Expression profiles of the identified hub genes were visualized using box plots in both the GSE55235 training cohort and the GSE55457 validation cohort (Figures 5A, 5B). Across the two datasets, *CXCL8* and *NFKBIA* exhibited decreased expression in osteoarthritic synovial tissue relative to normal controls, whereas MMP9 expression was elevated.

ROC curve analysis was performed in the GSE55235 training set (Figure 5C). In the GSE55235 training set, the AUCs for CXCL8, MMP9, and NFKBIA were 1.00, 0.97, and 1.00, respectively. In the independent GSE55457 validation set, CXCL8 and NFKBIA maintained AUCs > 0.7, whereas the AUC for MMP9 fell below 0.7, and therefore CXCL8 and NFKBIA were prioritized as the final candidate biomarkers (Figure 5D).

GSEA and immune infiltration analyses of CXCL8 and NFKBIA genes

To further characterize the biological pathways associated with *CXCL8* and *NFKBIA*, GSEA was performed. Both genes were significantly enriched in pathways related to immune response, inflammatory signaling, collagen metabolism, and additional regulatory processes (Figures 6A, 6B).

Immune cell infiltration analysis was conducted using the CIBERSORT algorithm. Statistically significant differences ($p < 0.05$) between OA and control samples were observed in plasma cells, resting cluster of differentiation 4 (CD4) memory T cells, Treg cells, activated natural killer cells, and mast cells (Figure 6C). Correlation patterns between hub gene expression and immune cell subsets were visualized using a heatmap (Figure 6D). *CXCL8* and *NFKBIA* expression levels showed positive correlations with resting CD4 memory T cells and activated mast cells, while negative correlations were observed with resting mast cells. In addition, NFKBIA expression was negatively correlated with M2 macrophages.

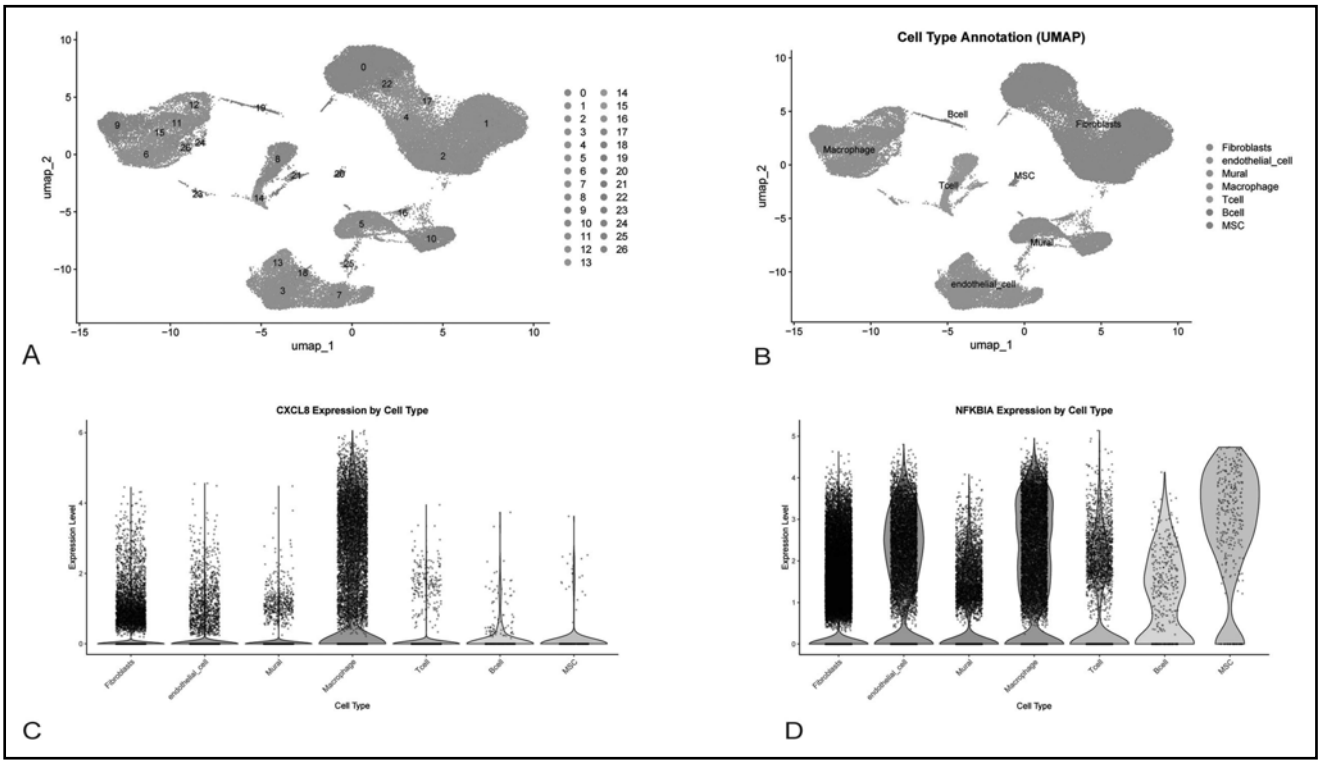

Fig. 7. Single-cell clustering and hub gene expression in synovial cell subsets
(A) Uniform manifold approximation and projection plot showing cell clusters in the GSE216651 single-cell dataset. (B) Uniform manifold approximation and projection plot showing annotated cell types. (C) Violin plot of CXCL8 expression across cell types. (D) Violin plot of NFKBIA expression across cell types.

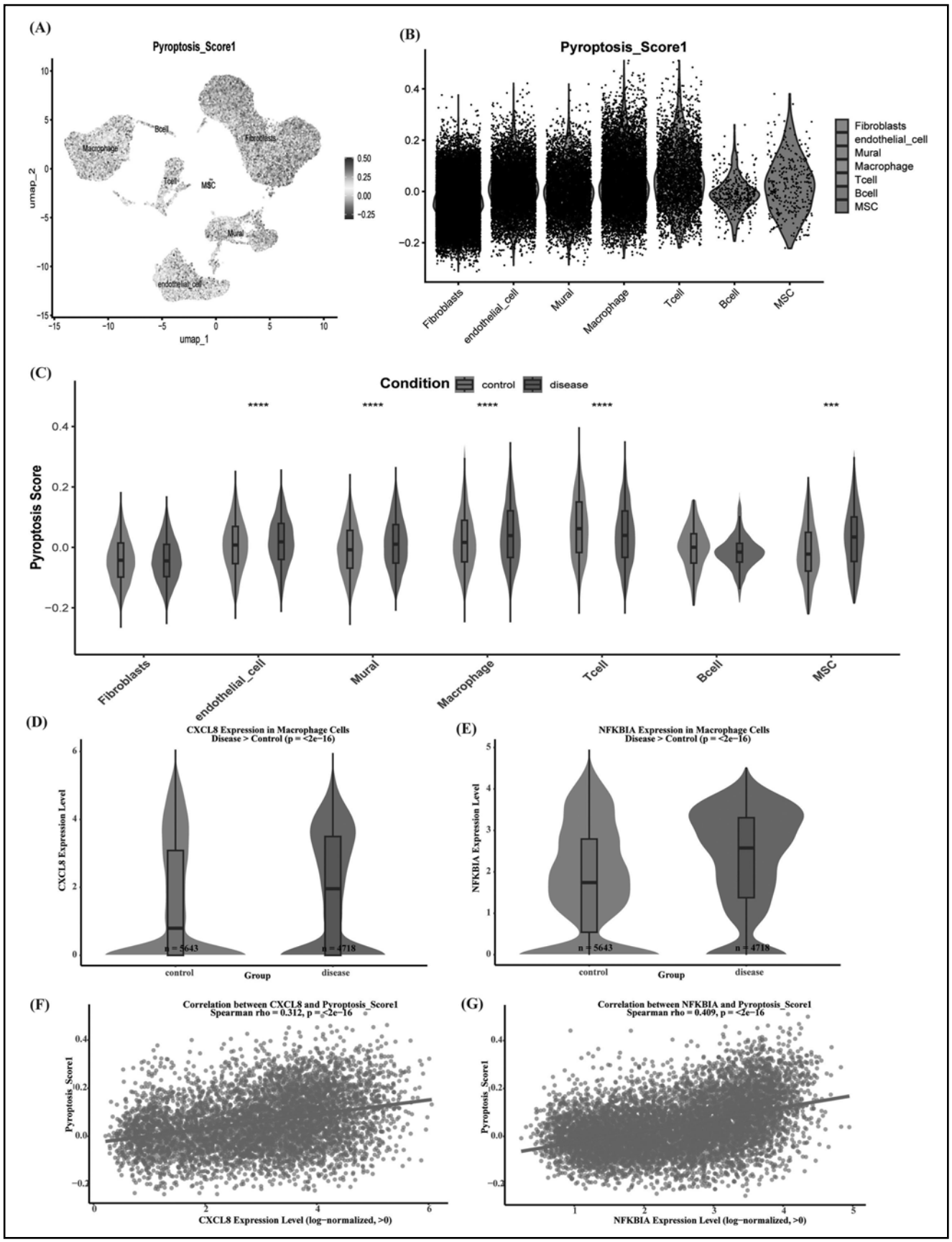

Fig. 8. Relationship between hub gene expression and pyroptosis in single-cell analysis
(A) Uniform manifold approximation and projection plot of pyroptosis scores. (B) Violin plot showing pyroptosis scores across cell types. (C) Comparison of pyroptosis scores between osteoarthritis and control groups across cell types. (D) Violin plot of CXCL8 expression in macrophages. (E) Violin plot of NFKBIA expression in macrophages. (F) Correlation between CXCL8 expression and pyroptosis score in macrophages. (G) Correlation between NFKBIA expression and pyroptosis score in macrophages.

Expression of hub gene expression across cell populations

Identifying the cellular origin of hub gene expression in OA synovial tissue is essential for understanding their potential contribution to disease progression. The published single-cell sequencing dataset GSE216651 was collected and reanalyzed. Dimensionality reduction and visualization were performed using the UMAP algorithm.

A total of 27 cellular clusters were identified (Figure 7A), which were subsequently annotated into seven distinct cell types based on established references (Figure 7B). In view of their strong diagnostic performance, the expression patterns of *CXCL8* and *NFKBIA* were further evaluated across these annotated cell populations. Violin plots showed that CXCL8 expression was concentrated in macrophages, whereas NFKBIA was detectable across several cell subsets with relatively higher expression in macrophages and fibroblasts (Figures 7C, 7D).

Relationship between hub genes and pyroptosis

Pyroptosis scores were calculated for each cell type within the single-cell dataset (Figures 8A, 8B). Among all annotated populations, macrophages exhibited the highest pyroptosis scores. Comparative analysis between OA and control samples revealed elevated pyroptosis scores in macrophages, pericytes, endothelial cells, and mesenchymal stem cells in the disease group (Figure 8C).

Given the prominent expression of *CXCL8* and *NFKBIA* in macrophages, together with the elevated pyroptosis activity observed in this cell population, macrophage-associated pyroptosis appears to be implicated in OA onset and progression. Macrophages were therefore selected for further subset analysis. Within this population, *CXCL8* and *NFKBIA* expression levels were higher in osteoarthritic samples than in controls (Figures 8D, 8E).

Within macrophages, CXCL8 and NFKBIA expression levels correlated positively with pyroptosis scores ($r = 0.312$ and $r = 0.409$, respectively; both $p < 0.05$) (Figures 8F, 8G).

DISCUSSION

OA has traditionally been characterized as a degenerative joint disorder. Increasing evidence, however, indicates that activation of the immune system and persistent intra-articular inflammation are central to disease initiation and progression (Shen and Jiang, 2025; Nedunchezhiyan *et al.* 2022). Synovial tissue, which contains a substantial population of immune cells, serves as a major site of inflammatory activity in OA (Ebata and Terkawi, 2023).

Pyroptosis is distinguished from other forms of programmed cell death by its pronounced pro-inflammatory properties. Multiple studies have documented heightened pyroptotic activity in OA synovial tissue (Yang *et al.* 2021), suggesting a potential role in amplifying local inflammatory responses. In light of these observations, systematic evaluation of pyroptosis-related mechanisms in OA, together with the identification of clinically relevant diagnostic biomarkers and therapeutic targets, warrants focused investigation.

This study integrated machine learning algorithms with bulk transcriptome and single cell RNA sequencing data to systematically screen for synovial pyroptosis related genes in OA. Through this analytical framework, candidate biomarkers were identified, and their potential involvement in relevant biological processes was further explored.

In the present study, GO and KEGG enrichment analyses were performed on 21 OA-related DEPRGs. The findings indicated that these genes are predominantly involved in immune responses and the regulation of inflammatory processes. GO functional annotation suggested that they contribute to the initiation and amplification of joint inflammation in OA, potentially through modulation of immune cell infiltration and inflammatory signal transduction pathways.

KEGG pathway analysis further demonstrated enrichment in key inflammatory signaling pathways, including the Toll-like receptor and TNF signaling pathways. These associations imply that the identified genes may influence OA onset and progression through their participation in these canonical inflammatory mechanisms.

Through the integration of Cytoscape-based network analysis and machine learning algorithms, three hub genes were identified: *CXCL8*, *MMP9*, and *NFKBIA*. ROC analysis performed in both the GSE55235 training cohort and the GSE55457 validation cohort demonstrated that *CXCL8* and *NFKBIA* each achieved AUC values greater than 0.7. These results support the potential utility of CXCL8 and NFKBIA as candidate diagnostic biomarkers for OA in public transcriptomic datasets.

CXCL8 is a member of the CXC chemokine family and encodes interleukin-8 (IL-8), a central mediator of inflammatory responses implicated in a range of inflammatory disorders. Elevated *CXCL8* expression has been reported in the cartilage tissue of patients with OA, where it promotes chondrocyte degradation through activation of the nuclear factor-κB (NF-κB) signaling pathway (Cai *et al.* 2025).

In abdominal aortic aneurysm, *CXCL8* has been shown to induce activation of the NLRP3 inflammasome, thereby triggering pyroptosis in vascular smooth muscle cells and exacerbating inflammatory injury within the aortic wall (Huang *et al.* 2025). In addition, IL-8 can initiate pyroptosis in human nasal epithelial cells through activation of the extracellular signal-regulated kinase (ERK) signaling pathway, contributing to glucocorticoid resistance in nasal polyp disease (Zhang *et al.* 2025). Collectively, these observations

support a potential role for *CXCL8* in inflammation mediated by pyroptotic mechanisms.

Analysis of publicly available transcriptomic datasets in the present study demonstrated lower *CXCL8* expression in OA synovial tissue compared to control samples in bulk transcriptome data, despite its strong diagnostic performance. This apparent reduction in synovial *CXCL8* expression contrasts with its established pro-inflammatory properties. To further clarify its cellular distribution, single-cell RNA sequencing analysis was performed, revealing that *CXCL8* expression was predominantly localized to macrophages.

Subsequent analysis restricted to the macrophage subset demonstrated higher *CXCL8* expression in osteoarthritic samples compared with controls. Moreover, macrophage-specific *CXCL8* expression exhibited a positive correlation with pyroptosis scores, aligning with its established pro-inflammatory and pro-pyroptotic characteristics. These findings indicate that bulk transcriptome data, which integrate signals from heterogeneous cell populations, may obscure cell type–specific expression patterns observed in the single-cell analysis. The apparent discrepancy in overall *CXCL8* expression between bulk and single-cell analyses may therefore reflect differences in cellular composition between disease and control groups.

GSEA and immune infiltration assessment further suggested that *CXCL8* may participate in OA progression through modulation of immune responses, inflammatory activity, and extracellular matrix metabolic imbalance. A positive correlation was also observed between *CXCL8* expression and activated mast cells, consistent with previous evidence implicating activated mast cells in OA pathophysiology (Gao *et al.* 2025).

Taken together, these observations support further investigation into whether targeted modulation of macrophage CXCL8 expression can influence OA associated inflammation and pyroptotic pathways in experimental models.

The *NFKBIA* gene encodes an inhibitory protein of NF-κB, which suppresses the NF-κB/Rel complex and thereby exerts anti-inflammatory effects (Zhou *et al.* 2023). NF-κB signaling is widely regarded as a pivotal pathway in inflammatory disorders, including OA. Dysregulated activation of NF-κB has been associated with chondrocyte catabolism and synovial inflammation, and pharmacologic or molecular inhibition of this pathway has been proposed as a potential therapeutic strategy for OA (Choi *et al.* 2019; Liu *et al.* 2023).

Experimental evidence indicates that overexpression of *NFKBIA* in OA synovial fibroblasts reduces the expression of matrix-degrading enzymes, such as matrix metallopeptidase 13 and ADAM metallopeptidase with thrombospondin type 1 motif 4, thereby alleviating extracellular matrix degradation in cartilage (Bondeson *et al.* 2007). In addition, disruption of alkylation repair homolog 5 (*ALKBH5*)-mediated stabilization of *NFKBIA* mRNA has been shown to enhance nuclear translocation of NF-κB p-p65, leading to exacerbation of osteoarthritic manifestations (Zhu *et al.* 2025). Collectively, these findings support a role for *NFKBIA* downregulation in contributing to OA progression in experimental models and transcriptomic analyses.

In the present study, bulk transcriptomic analysis of synovial tissue demonstrated lower *NFKBIA* expression in osteoarthritic samples compared with controls. This reduction was accompanied by favorable diagnostic performance, consistent with the established anti-inflammatory function of *NFKBIA* through inhibition of NF-κB signaling. However, single-cell RNA sequencing analysis revealed that within the macrophage subpopulation, NFKBIA expression was elevated in osteoarthritic samples relative to controls and showed a positive correlation with macrophage pyroptosis scores. At first glance, this observation appears to contrast with the concept that reduced *NFKBIA* expression facilitates OA progression.

This discrepancy may be attributable to the broad distribution of *NFKBIA* across multiple synovial cell types, with bulk transcriptomic data representing an aggregate signal derived from heterogeneous cellular populations. The overall decrease observed in bulk analysis may reflect widespread downregulation in most cell subsets. In contrast, macrophages, recognized as key pro-inflammatory effectors in OA (Qi *et al.* 2024), may undergo pronounced NF-κB activation and pyroptotic activity. Such activation could trigger a negative feedback response, leading to compensatory upregulation of NFKBIA expression within this cell population as a potential mechanism to limit excessive inflammatory signaling.

GSEA and immune infiltration analyses further suggested that *NFKBIA* may regulate osteoarthritic inflammation through effects on immune cell populations, such as B lymphocytes and other leukocytes, thereby contributing to disease initiation and progression. Future investigation is warranted to delineate the cell type–specific functions of *NFKBIA* in OA, particularly within synovial macrophages and fibroblast-like synoviocytes.

Several limitations should be acknowledged. First, the identification of OA associated pyroptosis related signature genes was derived exclusively from bioinformatics analyses and has not been corroborated by in vivo or in vitro experimental validation so the proposed biomarkers should be regarded as preliminary and hypothesis-generating. Second, the sequencing datasets included relatively small sample sizes, which may limit the generalizability of the findings and contribute to optimistic performance estimates in the machine learning models. Third, gene sets for OA RGs and pyroptosis RGs were obtained from public databases and may contain annotation bias or noise, which could influence the selection of DEPRGs. Confirmation in larger, independent cohorts is therefore necessary to substantiate these conclusions.

In summary, comprehensive bioinformatics analyses identified *CXCL8* and *NFKBIA* as synovium-associated pyroptosis signature genes in OA. Dysregulated expression of these genes in osteoarthritic synovial tissue may be associated with disease progression through modulation of pyroptotic activity, thereby affecting inflammatory responses and immune cell infiltration. These findings enhance understanding of pyroptosis-related molecular mechanisms in OA synovial tissue and may inform the identification of macrophage-centered candidate diagnostic markers and potential therapeutic targets, particularly involving CXCL8- and NFKBIA associated pathways. Further studies are warranted to validate these biomarkers in clinical settings and to elucidate their underlying mechanisms using in vivo and in vitro experimental models.

DECLARATIONS

Ethics approval and consent to participate

The patients involved in the public database have obtained ethical approval. Users can download relevant data for free for research and publish relevant articles. Our study is based on open source data, so there are no ethical issues and other conflicts of interest.

Consent for publication

Not applicable

Competing interests

The authors declare that they have no competing interests.

Funding

No external funding received to conduct this study.

Availability of data and materials

All data generated or analyzed during this study are included in this article. Further enquiries can be directed to the corresponding author.

Acknowledgments

We would like to acknowledge the hard and dedicated work of all the staff that implemented the intervention and evaluation components of the study.

Authors' contributions

Conception and design of the research: Jun-Lin Chen
Acquisition of data: Rui-Hai Ya
Analysis and interpretation of the data: Yan-Hui Suo
Statistical analysis: Yan-Hui Suo
Writing of the manuscript: Jun-Lin Chen
Critical revision of the manuscript for intellectual content: Rui-Hai Ya
All authors read and approved the final draft.

REFERENCES

1 Bondeson J, Lauder S, Wainwright S, Amos N, Evans A, Hughes C, et al. (2007). Adenoviral gene transfer of the endogenous inhibitor IκBα into human osteoarthritis synovial fibroblasts demonstrates that several matrix metalloproteinases and aggrecanases are nuclear factor-κB-dependent. J Rheumatol. **34**(3): 523–533. DOI: 10.3899/jrheum.061064.
2 Cai D, Hu Z, Zhu Y, Zhang H, Liu X, Wang L, et al. (2025). CXCL8 and GZMB genes promote cartilaginous and synovial lesion formation via NF-κB and MAPK signaling pathways in Kaschin-Beck disease. Biochim Biophys Acta Mol Basis Dis. **1871**(7): 167921. DOI: 10.1016/j.bbadis.2025.167921.
3 Chen X, Song Y (2025). Mechanistic insights into celastrol's anti-pyroptosis effects in osteoarthritis via SIRT2 upregulation. Mediators Inflamm. **2025**: 5676471. DOI: 10.1155/2025/5676471.
4 Choi MC, Jo J, Park J, Kang HK, Park Y (2019). NF-κB signaling pathways in osteoarthritic cartilage destruction. Cells. **8**(7): 734. DOI: 10.3390/cells8070734.
5 Cui Y, Wang YL, Wei J, Huang GY, Li ZH, Zhang L, et al. (2025). Annual advances in osteoarthritis research 2024. Natl Med J China. **105**(21): 1757–1762. DOI: 10.3760/cma.j.cn112137-20241231-02969.
6 Ebata T, Terkawi MA (2023). Noncanonical pyroptosis triggered by macrophage-derived extracellular vesicles in chondrocytes leading to cartilage catabolism in osteoarthritis. Arthritis Rheumatol. **75**(8): 1358–1369. DOI: 10.1002/art.42581.
7 Expert Group of Chinese Guidelines for Diagnosis and Treatment of Osteoarthritis, The Pain Disease Branch of the Chinese Aging Well Association (2024). Chinese guidelines for diagnosis and treatment of osteoarthritis (2024 edition). Chin J Painol. **20**(3): 323–338. DOI: 10.3760/cma.j.cn101658-20240618-00074.
8 Gao J, Zhao D, Nouri HR, Wang Y, Li S, Chen R, et al. (2025). Transcriptional regulation of mouse mast cell differentiation and the role of human lung mast cells in airway inflammation. Immunol Rev. **331**(1): e70026. DOI: 10.1111/imr.13024.
9 Glyn-Jones S, Palmer AJ, Agricola R, Price AJ, Vincent TL, Weinans H, et al. (2015). Osteoarthritis. Lancet. **386**(9991): 376–387. DOI: 10.1016/S0140-6736(14)60802-3.
10 Huang Y, Xie X, Huang G, Liu W, Chen J, Li Y, et al. (2025). CXCL8 upregulation mediates inflammatory cell infiltration and accelerates abdominal aortic aneurysm progression. Sci Prog. **108**(1): 368504251328754. DOI: 10.1177/00368504241328754.
11 Kuang S, Sheng W, Meng J, Zhang W, Li X, Wang Y, et al. (2024). Pyroptosis-related crosstalk in osteoarthritis: macrophages, fibroblast-like synoviocytes and chondrocytes. J Orthop Translat. **47**: 223–234. DOI: 10.1016/j.jot.2024.02.004.
12 Litwic A, Edwards MH, Dennison EM, Cooper C (2013). Epidemiology and burden of osteoarthritis. Br Med Bull. **105**: 185–199. DOI: 10.1093/bmb/lds038.
13 Liu J, Jia S, Yang Y, Li M, Zhao L, Wang J, et al. (2023). Exercise-induced meteorin-like protects chondrocytes against inflammation and pyroptosis in osteoarthritis by inhibiting PI3K/Akt/NF-κB and NLRP3/caspase-1/GSDMD signaling. Biomed Pharmacother. **158**: 114118. DOI: 10.1016/j.biopha.2022.114118.
14 Mathiessen A, Conaghan PG (2017). Synovitis in osteoarthritis: current understanding with therapeutic implications. Arthritis Res Ther. **19**(1): 18. DOI: 10.1186/s13075-017-1229-9.
15 Motta F, Barone E, Sica A, Selmi C (2023). Inflammaging and osteoarthritis. Clin Rev Allergy Immunol. **64**(2): 222–238. DOI: 10.1007/s12016-021-08884-6.
16 Nedunchezhiyan U, Varughese I, Sun AR, Zreiqat H, Pavelka K, Kandel RA, et al. (2022). Obesity, inflammation, and immune system in osteoarthritis. Front Immunol. **13**: 907750. DOI: 10.3389/fimmu.2022.907750.
17 Qi W, Jin L, Huang S, Li C, Xu M, Li Y, et al. (2024). Modulating synovial macrophage pyroptosis and mitophagy interactions to mitigate osteoarthritis progression using functionalized nanoparticles. Acta Biomater. **181**: 425–439. DOI: 10.1016/j.actbio.2023.12.050.
18 Sanchez-Lopez E, Coras R (2022). Synovial inflammation in osteoarthritis progression. Nat Rev Rheumatol. **18**(5): 258–275. DOI: 10.1038/s41584-022-00749-9.

19 Shen T, Jiang Q (2025). The role of immune cells in the pathogenesis and progression of osteoarthritis warrants attention. Natl Med J China. **105**(35): 3043–3048. DOI: 10.3760/cma.j.cn112137-20250217-00358.
20 Siddiq MAB, Oo WM, Hunter DJ (2024). New therapeutic strategies in osteoarthritis. Joint Bone Spine. **91**(6): 105739. DOI: 10.1016/j.jbspin.2024.105739.
21 Vasudevan SO, Behl B, Rathinam VA (2023). Pyroptosis-induced inflammation and tissue damage. Semin Immunol. **69**: 101781. DOI: 10.1016/j.smim.2023.101781.
22 Yang J, Hu S, Bian Y, Yao J, Wang D, Liu X, et al. (2021). Targeting cell death: pyroptosis, ferroptosis, apoptosis and necroptosis in osteoarthritis. Front Cell Dev Biol. **9**: 789948. DOI: 10.3389/fcell.2021.789948.
23 Yu JL, Wang WB (2025). Application of artificial intelligence in the diagnosis, progress, and treatment of osteoarthritis. Chin J Anat Clin. **30**(10): 708–712. DOI: 10.3760/cma.j.cn101202-20241229-00389.
24 Zhang W, Lei Y, Zhang T, Liu J, Li F, Chen G, et al. (2025). IL-8 promotes pyroptosis through ERK pathway and mediates glucocorticoid resistance in chronic rhinosinusitis with nasal polyps. Inflamm Res. **74**(1): 20. DOI: 10.1007/s00011-024-01780-3.
25 Zhou J, Huang J, Li Z, Wang S, Liu Y, Zhang Y, et al. (2023). Identification of aging-related biomarkers and immune infiltration characteristics in osteoarthritis based on bioinformatics analysis and machine learning. Front Immunol. **14**: 1168780. DOI: 10.3389/fimmu.2023.1168780.
26 Zhu C, Liu G, Zhou W, Chen Z, Wang H, Li Y, et al. (2025). tRF16 affects NFKBIA stability and promotes osteoarthritis progression by regulating ALKBH5 expression in an m6A-dependent manner. Commun Biol. **8**(1): 868. DOI: 10.1038/s42003-025-07562-9.